Local Motions of *cis*-1,4-Polybutadiene in the Melt. A Quasielastic Neutron-Scattering Study

Toshiji Kanaya,*,† Keisuke Kaji,† and Kazuhiko Inoue‡

Institute for Chemical Research, Kyoto University, Uji, Kyoto-fu 611, Japan, and Department of Nuclear Engineering, Hokkaido University, Sapporo 060, Japan

Received August 1, 1990; Revised Manuscript Received October 22, 1990

ABSTRACT: Local motions of *cis*-1,4-polybutadiene in the melt have been investigated by quasielastic neutron scattering in the time range 10^{-13} to 10^{-10} s. We found two modes in this time range. The characteristic time of the faster mode is on the order of 10^{-12} s, and the activation energy is $\simeq$0.5 kcal/mol. On the other hand, the slower mode has a characteristic time of about 5×10^{-11} s with an activation energy of $\simeq$2.5 kcal/mol, which almost corresponds to the height of one energy barrier separating rotational isomeric states (2–3 kcal/mol). The faster and slower modes are assigned to damped vibrational motion and local conformational transition, respectively. The latter is analyzed in terms of a jump diffusion model with the damped vibrational motions on the jump sites. The physical picture of the model is very similar to the results of the dynamic simulation by Helfand and co-workers, which have showed that isolated conformational transitions occur as well as cooperative transitions. The observed conformational transition rate is compared with the Kramers' rate theory, and the spatial scales of the motions are discussed based on the molecular structure of *cis*-1,4-polybutadiene.

Introduction

In polymer chains, conformational transitions between rotational isomeric states are fundamental to the understanding of many of the rapid relaxation processes. These local motions in solutions and melts have been studied by many techniques, e.g., NMR,[1] dielectric relaxation,[2,3] ultrasonic attenuation,[4] fluorescence depolarization,[5-7] and excimer fluorescence.[8] Crankshaftlike motions such as Schatzki crankshaft[9] or three-bond motion[10] were considered to be the most reasonable explanation of the local motions. However, recent important progress in this field has provided an argument against the crankshaftlike motions. Helfand and co-workers[11] have made computer simulations by employing a realistic polymer chain involving bond rotation, bond angle bending, and bond length stretching and found that the activation energy for the conformational transition is approximately equal to the height of one energy barrier separating the rotational isomeric states. This result is also supported by some experiments.[2,3,8] On the other hand, the crankshaftlike motions require activation energies larger than the height of one barrier, because several bonds must be in the activated state almost simultaneously. The computer simulation has also indicated that cooperative transitions as well as isolated transitions occur. The major manifestation of the former is the counterrotational transitions of two second neighboring bonds separated by a trans bond. A key point to the understanding of the conformational transitions is to study the reaction coordinate in the neighborhood of the transition state. Skolnick and Helfand[12] have extended the Kramers' reaction rate theory to multidimensional systems and shown that the reaction coordinate is a localized mode; i.e., the rotational motion of the transforming bond is accompanied by motions in neighboring bonds (distortions of neighboring degrees of freedom), but these motions diminish with distance. To distort neighboring degrees of freedom while keeping the motion localized, the softest degrees of freedom or bond rotations are the most favorable. The reaction path for the conformational transition is the steepest descent from the top of the barrier (activated state) to a local equilibrium position of the rotational isomeric states. This process is kinematically controlled so that it branches into various channels. Therefore, some transitions occur individually and some cooperatively.

Our attention is focused on the mechanism of the local conformational transitions in polymer chains. As shown in the computer simulation,[11] the conformational transitions are assisted by distortions in a polymer chain through vibrational motions, especially bond rotations or torsional vibrations. We are also interested in the vibrational motions, which are probably damped due to thermal agitations or high friction in both solutions and melts. These motions are faster than the local conformational transitions. Quasielastic neutron scattering is one of the most appropriate methods to prove these motions in the time range 10^{-13}–10^{-10} s and gives direct spatial information on the motions because the measurements are made as functions of both energy and momentum transfers.

In this work, we carry out quasielastic neutron-scattering measurements on *cis*-1,4-polybutadienes in the melt. Higgins et al.[14] have studied the local chain dynamics of a number of polymers in the melts by quasielastic neutron scattering. They are concerned with slow segmental motions, which are described by the Rouse model. On the other hand, our main purpose is to investigate the local conformational transitions and the damped vibrational motions that assist the transitions. These processes occur in the time range 10^{-13}–10^{-9} s and are faster than the segmental motions. In the measurements, we have employed the two quasielastic neutron-scattering spectrometers, LAM-40 and LAM-80. Using these two spectrometers we can cover the energy range 0.01–10 meV, which corresponds to the time range 4.1×10^{-10}–4.1×10^{-13} s.[15] We find two modes of motion in this time range. The faster mode is assigned to the damped torsional vibration (bond rotation). The slower mode can be related to the local conformational transitions and analyzed in terms of a jump diffusion model with the damped vibrational motions. The results of the analysis are discussed based on the Kramers' rate theory and molecular structure of *cis*-1,4-polybutadiene.

† Kyoto University.
‡ Hokkaido University.

0024-9297/91/2224-1826$02.50/0

Experimental Section

Samples. The samples used for the scattering experiments are *cis*-1,4-polybutadienes (PB) with molecular weights of 8.1×10^5 and 2.7×10^5, which were kindly supplied by the Japan Synthetic Rubber Co., Ltd., and purified by precipitating from a toluene solution into excess methanol. The contents of cis, trans, and vinyl in these samples were determined by IR measurements as 95.7, 2.0, and 2.3% and 94.8, 2.3, and 2.9%, respectively. For neutron-scattering measurements, PB was coated on the outer surface of a hollow aluminum cylinder 140 mm high, 13.8 mm in diameter, and 0.25 mm thick. The thickness of the coated sample was controlled to be less than 0.1 mm so that multiple scattering would be suppressed below 10%.

Neutron-Scattering Measurements. Quasielastic neutron scattering measurements were performed with the inverted geometry time-of-flight (TOF) spectrometers LAM-40 and LAM-80[16] installed at the pulsed spallation cold neutron source in the National Laboratory for High Energy Physics (KEK), Tsukuba, Japan. In operation of these spectrometers, pulsed cold neutrons with a wide energy distribution are incident on a sample, and the scattered neutrons with fixed energy (4.59 and 1.87 meV for LAM-40 and LAM-80, respectively) are selected by a PG(002) crystal analyzer mirror and a Be filter and detected by ^{3}He counters at several scattering angles. The energy resolutions evaluated from the full width of the elastic peaks are ~0.2 V and ~0.01 meV, and the energy windows are below 10 and 0.5 meV, respectively. The lengths of the scattering vector Q at the elastic position range from 0.2 to 2.6 Å^{-1} and from 0.2 to 1.8 Å^{-1} for LAM-40 and LAM-80, respectively. The neutron-scattering measurements on PB were carried out at 23, 45, 60, 80, 100, 120, and 140 °C, enough above the melting temperature of PB of about 2 °C.[17]

Data Analysis. After making corrections for background, counter efficiency, and the incident neutron spectrum, the observed TOF spectrum was converted to a differential scattering cross section $\partial^2\sigma/\partial\Omega\partial E$, which is defined as the probability that an incident neutron with energy E_0 is scattered into a solid angle $\partial\Omega$ and in an energy interval between E and $E + \partial E$. In the measurements of PB, the observed differential scattering cross section is mainly dominated by incoherent scattering of hydrogen atoms, because PB contains only H and C atoms, and the incoherent atomic scattering cross section of hydrogen is much larger than the incoherent and coherent atomic scattering cross sections of carbon as well as the coherent one of hydrogen.[18] Therefore, the observed differential scattering cross section can be approximated to the incoherent dynamic scattering law $S_{inc}(Q,\omega)$ through

$$\frac{\partial^2\sigma_{inc}}{\partial\Omega\partial E} \simeq \frac{k_1}{k_0}(\langle b^2\rangle - \langle b\rangle^2)S_{inc}(Q,\omega) \quad (1)$$

where k_0 and k_1 are the lengths of the wave vectors of incident and scattered neutrons k_0 and k_1, respectively. Q is the length of the scattering vector $\mathbf{Q}$ defined as $Q = k_0 - k_1$. b is the scattering length of the hydrogen atom and $4\pi(\langle b^2\rangle - \langle b\rangle^2)$ corresponds to the incoherent atomic cross section. Using eq 1, we calculated the incoherent dynamic scattering law $S_{inc}(Q,\omega)$.

Analysis of the observed dynamic scattering laws was carried out by curve fitting with model functions using the computer codes QUESA40 and QUESA80.[16] It is noted that the curve fit is not made in energy space but in TOF space in the codes. The energy ranges used for the curve fit ΔE ($=\hbar\omega$) were −2.2 to 9.5 and −0.25 to 0.25 meV for LAM-40 and LAM-80 data, respectively.

Results and Discussion

As described in the last section, the experiments were performed by two spectrometers. We will first discuss the results obtained by LAM-40. On the basis of this discussion, the results of LAM-80 will then be analyzed and discussed.

Damped Vibrational Motions from LAM-40 Data. Results of LAM-40 Measurements. The observed quasielastic neutron-scattering spectra $S_{inc}(Q,\omega)$ at Q = 1.76 Å^{-1} of molten PB with a molecular weight of 8.1×10^5 are shown in Figure 1 as a function of temperature from 23 to 100 °C. Each spectrum consists of elastic scattering and a broad quasielastic scattering. Here it should be noted that the elastic peak is only apparent because the samples are liquid with no fixed centers of mass. All the motions slower than the resolution of the LAM-40 spectrometer are included in the elastic peak. The appearance of an elastic component means that the observed motion is restricted in a finite volume[19] within the time corresponding to the the resolution of the spectrometer. The scattering spectra of PB with a molecular weight of 2.7×10^5 are identical with those of PB with a molecular weight of 8.1×10^5 within experimental error. In order to separate the elastic and quasielastic scattering components quantitatively, it was first tried to fit the observed spectra with a model function given by the sum of a δ-function and a Lorentzian. However, the agreement was not good between the observed and calculated spectra because the observed ones have a very broad quasielastic component. Such a broad component is often treated as inelastic flat background,[20] but it is impossible to do so in the present spectra because the shape of the broad component is Lorentzian-like in the energy range below 10 meV. Therefore, we have again fitted with a model function given by the sum of a δ-function and two Lorentzians

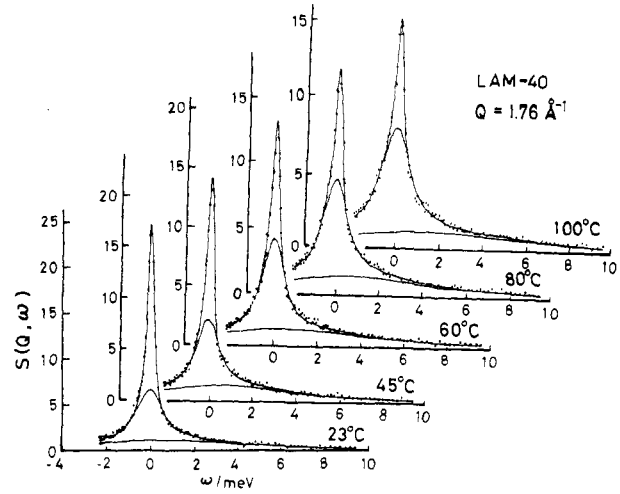

Figure 1. Quasielastic neutron-scattering spectra at Q = 1.76 Å^{-1} of molten *cis*-1,4-polybutadiene measured by LAM-40 as a function of temperature from 23 to 100 °C. Solid lines represent the fitting results including elastic and two quasielastic components.

$$S_{inc}(Q,\omega) = C(Q)[\{1 - A_{1n}(Q) - A_{1b}(A)\}\delta(\omega) + A_{1n}(Q)L(Q,\omega,\Gamma_{1n}) + A_{1b}(Q)L(Q,\omega,\Gamma_{1b})] \quad (2)$$

where $C(Q)$ is a constant including parameters of LAM-40, $L(Q,\omega,\Gamma_i)$ (i = 1n and 1b) a normalized Lorentzian with half-width at half-maximum (hwhm) Γ_i, $A_i(Q)$ (i = 1n and 1b) the fraction of the corresponding Lorentzian, and $\delta(\omega)$ a δ-function. This function gives an excellent agreement with the experimental spectra. The solid lines in Figure 1 show the results of the fit. There is a possibility that other mathematical functions would fit in with the observed spectra. However, at the present stage, we have no reasons to judge which function showing an excellent fit has a reasonable physical picture. Therefore, we at first employ the results of the fitting with eq 2 to clarify the nature of the motion.

The hwhm Γ_{1b} and Γ_{1n}, or the inverse of characteristic times τ_{1b} and τ_{1n} of the broad and narrow quasielastic components for PB at 45 °C, are plotted as a function of Q in Figure 2. The Q dependences are almost identical for both Γ_{1b} and Γ_{1n}; they are independent of Q below ca.

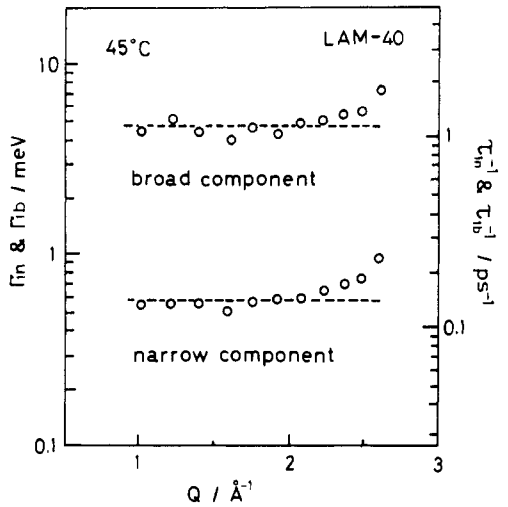

Figure 2. Q dependences of half-width at half-maximum (hwhm) of the broad and narrow quasielastic components Γ_{1b} and Γ_{1n} obtained by LAM-40 at 45 °C. Γ_{1b} and Γ_{1n} correspond to the inverses of characteristic times τ_{1b} and τ_{1n}, respectively.

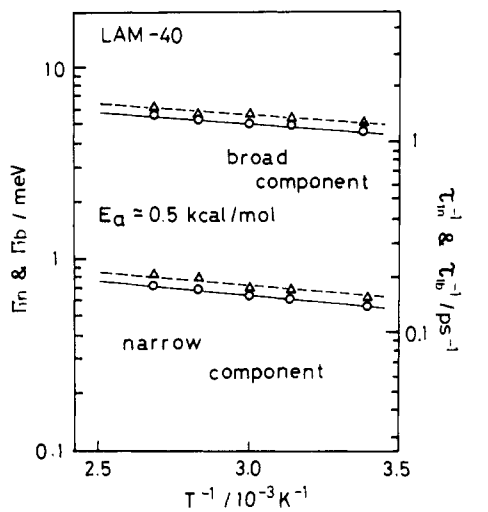

Figure 3. Temperature dependences of half-width at half-maximum (hwhm) of the broad and narrow quasielastic components Γ_{1b} and Γ_{1n} obtained by LAM-40. Γ_{1b} and Γ_{1n} correspond to the inverses of characteristic times τ_{1b} and τ_{1n}, respectively: (○) Q = 2.07 Å^{-1}; (△) Q = 2.35 Å^{-1}.

2.2 Å^{-1} and increase slightly with Q above 2.2 Å^{-1}. The same Q dependence suggests that the two components belong to a single mode of motion, which is very localized. The time scales of the broad (faster) and narrow (slower) components evaluated from the characteristic times τ_{1b}, ($=\Gamma_{1b}^{-1}$) and τ_{1n} ($=\Gamma_{1n}^{-1}$) are about 0.7 and 5 ps, respectively. These values are too fast for conformational transitions.[11,12]

The temperature dependences of Γ_{1b} and Γ_{1n} are shown in Figure 3, where they are plotted in the Arrhenius fashion. The very weak temperature dependences give an activation energy of $E_a \simeq 0.5$ kcal/mol for both components in the whole Q range measured. This also suggests that the broad (faster) and narrow (slower) components belong to a single mode. Some models have been proposed for localized motion or damped vibrational motion.[19,20] Scattering laws for such models are often given by a δ-function plus some Lorentzians, similar to the function used in the fitting (eq 2).

Damped Vibrational Motions. A problem that we have to consider is what is the mode observed by LAM-40. It is considered that the motion involves no local conformational transitions between rotational isomeric states

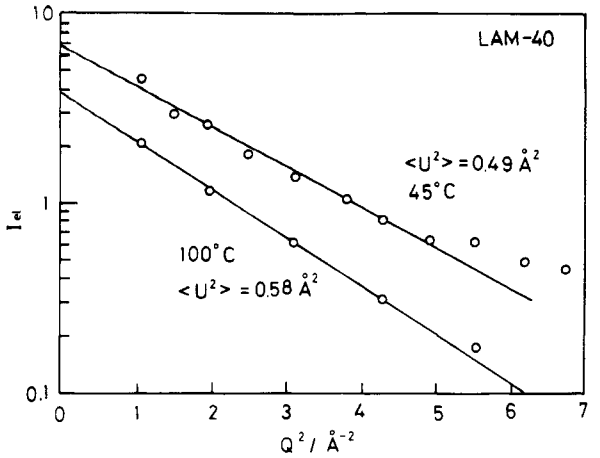

Figure 4. Logarithm of elastic scattering intensity as a function of Q^2 for *cis*-1,4-polybutadiene measured by LAM-40 at 45 and 100 °C. Mean-square amplitudes of the damped vibrations $\langle U^2 \rangle$ are 0.49 and 0.58 Å^2 for 45 and 100 °C, respectively. Values of $\langle U^2 \rangle$ are listed in Table I.

(RIS) because (i) the activation energy E_a ($\simeq$0.5 kcal/mol) is too small for the conformational transitions, which require at least one barrier height separating RIS (2–3 kcal/mol), (ii) both Γ_{1b} and Γ_{1n} are almost independent of Q, suggesting that the motion is very localized, and (iii) the characteristic times τ_{1b} and τ_{1n} are too fast for conformational transitions comparing with the computer simulation[11] and the rate theory.[12] It is considered that there are two possibilities for this restricted motion: (a) damped vibrational motion and (b) diffusive motion in a finite volume (a cage). However, it seems difficult to distinguish these two possibilities from the observed scattering spectra because both the motions are very similar to each other under the condition of strong damping. Buchenau et al.[22] have observed a very broad quasielastic scattering component ($\Gamma \simeq 4$ meV) in molten polyethylene (PE), which is the same order with the average of Γ_{1b} and Γ_{1n} observed in PB. The broad components of PE were satisfactorily described in the same quality of fit by either of two different pictures of restricted motion, i.e., quasiharmonic vibrations and diffusion within a sphere. The former and the latter have physical pictures similar to the damped vibrational motion and the diffusive motion in a finite volume, respectively. Even though we carry out curve fitting with these functions, it would be impossible to judge which picture is appropriate for the motion observed by LAM-40. In order to specify the mode of the motion by the curve fitting, we should employ a more realistic model constructed from detailed geometrical information on the motion. Unfortunately, less information makes it impossible. Generally speaking, low-frequency vibrational motions or librations in this time range are usually observed in the glassy states,[23] and they are probably damped by thermal agitations in the molten states. Further, the activation energy of this motion (E_a $\sim$ 0.5 kcal/mol) is too small for diffusive motions. In the present stage, therefore, we assign the mode to a damped vibrational motion.

The spatial scale of the motion is evaluated assuming that the Q dependence of the elastic scattering intensity can be described by the Debye–Waller function; i.e., $I_{el} \sim \exp(-\langle U^2 \rangle Q^2)$ where $\langle U^2 \rangle$ is the mean-square amplitude of the damped vibrational motion. In Figure 4, log I_{el} is plotted against Q^2 for PB at 45 and 100 °C. A linear relationship between log I_{el} and Q^2 is obtained in the Q range below 2.2 Å^{-1}, while it slightly deviates above 2.2 Å^{-1}. The mean-square amplitude $\langle U^2 \rangle$ was evaluated from

Table I
Parameters of the Jump Diffusion Model for the Local Conformational Transitions Determined from LAM-40 and LAM-80 Data

T/°C	$\langle U^2\rangle$/ Å^2	$\langle l^2\rangle^{1/2}$/ Å[a]	τ_0/ps[b]	$D/10^2$Å^2 ps^{-1}[c]	$\langle\Delta\phi\rangle$/ deg	τ_K/ps[d]
23	0.44	(3.71)	81.0	(4.5)	33	102
45	0.49				35	72.6
60	0.51	2.31	48.6	1.8	36	59.1
80	0.55	2.12	35.6	2.1	38	46.0
100	0.58	1.76	28.9	1.8	39	36.8
120	0.62	1.43	22.4	1.5	41	30.2
140	0.66	1.85	21.2	2.7	42	25.3

[a] Value of $\langle l^2\rangle^{1/2}$ calculated from molecular structure is 2.03 Å. [b] Activation energy of τ_0 (E^*) is 2.9 kcal/mol. [c] Calculated from $D = \langle l^2\rangle/6\tau_0$. [d] Calculated from Kramers' rate theory.

the slope of the straight line in Figure 4 to be 0.49 and 0.58 Å^2 for 45 and 100 °C, respectively. The results are summarized in Table I. We will later discuss the values of $\langle U^2\rangle$ based on the molecular structure of PB. The main contribution to $\langle U^2\rangle$ is probably from the torsional vibrations of the C–C bond (bond rotation) because it is the softest mode, and the amplitude of hydrogen atom displacement is larger than those of other modes. The potential shape for the torsional vibration can be described by a quadratic form in the crystalline state. However, it is natural to consider that the shape in the molten state is distorted by strain due to the local conformational transition and/or surrounding polymer chains. The activation energy of the damped vibrational motion ($\simeq$0.5 kcal/mol) should reflect the low barrier caused by the distortion.

Local Conformational Transition from LAM-80 Data. Results of LAM-80 Measurements. The spectrometer LAM-80 is accessible to the energy range 0.01–0.5 meV, which corresponds to the time range 4.1 × 10^{-10}–8.3 × 10^{-12} s. Therefore, we can observe further slower motions compared with LAM-40 measurements. The observed quasielastic scattering spectra at Q = 1.23 Å^{-1} of PB are shown in Figure 5 as a function of temperature from 23 to 100 °C. A new very narrow quasielastic component is observed in the spectra. This component cannot be detected by LAM-40 because it is included in the resolution function (elastic component). The elastic component observed in the LAM-80 spectra originates from slower modes than the resolution of LAM-80. These spectra were fitted in with the following model function using the parameters of $A_{1n}(Q)$, $A_{1b}(Q)$, Γ_{1n}, and Γ_{1b} determined in the LAM-40 spectra

$$S_{inc}(Q,\omega) = C'(Q)[\{1 - A_{2c}(Q) - A_{1n}(Q) - A_{1b}(Q)\}\delta(\omega) + A_{2c}(Q)\,L(Q,\omega,\Gamma_{2c}) + A_{1n}(Q)\,L(Q,\omega,\Gamma_{1n}) + A_{1b}(Q)L(Q,\omega,\Gamma_{1b})] \quad (3)$$

where $C'(Q)$ is a constant including parameters of LAM-80, and others have the same meaning with eq 2. In eq 3, a new term $A_{2c}(Q)\,L(Q,\omega,\Gamma_{2c})$ is introduced to represent the new narrow component. The fitting results are shown by solid curves in Figure 5 where the almost flat lines represent the sum of the two quasielastic components observed by LAM-40. The Arrhenius plots of hwhm of the new narrow component Γ_{2c} at Q = 1.23 and 1.73 Å^{-1} are shown in Figure 6a. The activation energies evaluated from the slope are 2.5 kcal/mol for both Q values. This value corresponds nearly to the height of one energy barrier separating RIS. It means that the new quasielastic component can be related to the local conformational transitions. As is seen in Figure 6a and will be shown later in detail, the absolute value of Γ_{2c} depends on Q in contrast to the independence of Γ_{1n} and Γ_{1b}.

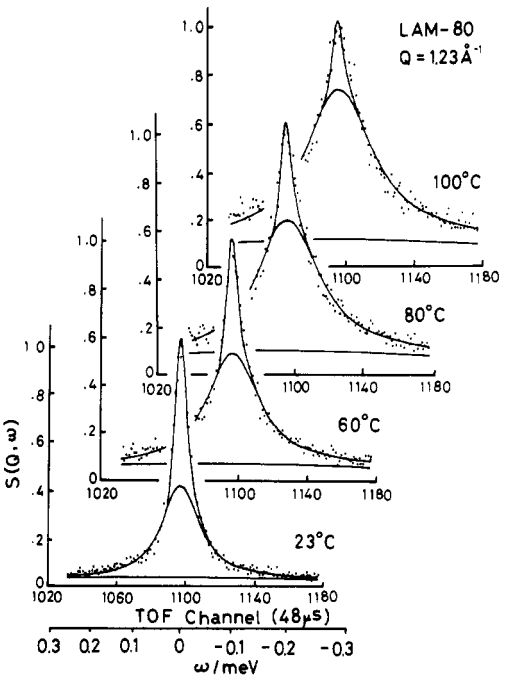

Figure 5. Quasielastic neutron scattering spectra at Q = 1.23 Å^{-1} of molten *cis*-1,4-polybutadiene measured by LAM-80 as a function of temperature from 23 to 100 °C. Solid lines represent the fitting results including elastic and quasielastic components. The almost flat lines represent the sum of the two quasielastic components observed by LAM-40.

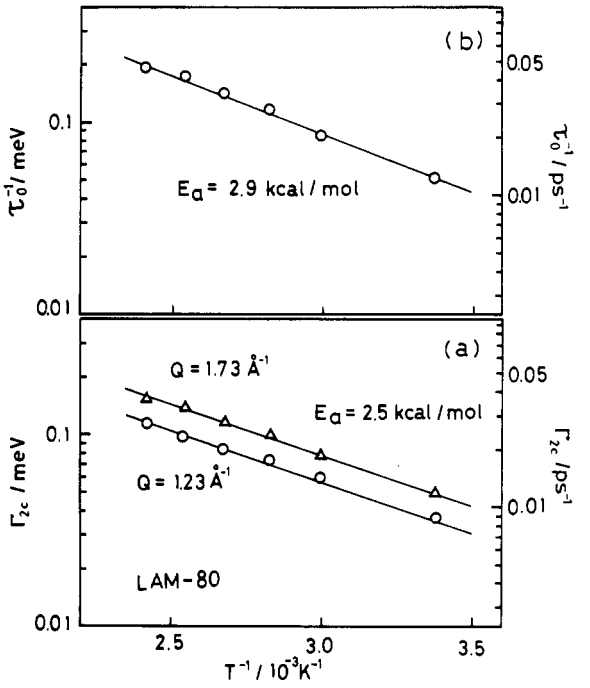

Figure 6. (a) Temperature dependence of half-width at half-maximum (hwhm) of the quasielastic component Γ_{2c} revealed by LAM-80. The activation energy of Γ_{2c} is 2.5 kcal/mol: (○) Q = 1.23 Å^{-1}; (△) Q = 1.73 Å^{-1}. (b) Temperature dependence of the inverse of the rest time τ_0, which corresponds to the local conformational transition rates. The activation energy of τ_0 is 2.9 kcal/mol.

Jump Diffusion Model with Damped Vibrational Motions. A Model for Local Conformational Transition. For the local conformational transition, we adopt a jump diffusion model with the damped vibrational motions by taking into account the results of the computer simulation by Helfand.[11] An outline of the model and some of the assumptions are given in the following.

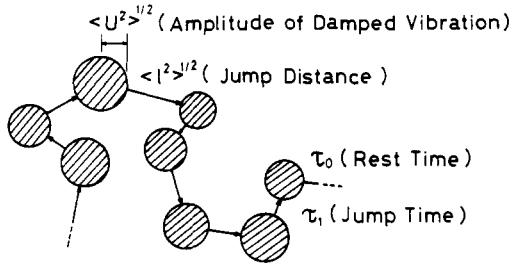

Figure 7. Schematic sketch of the jump diffusion model with damped vibrational motions. It is assumed that $\tau_0 \gg \tau_1$ in the present analysis, so that τ_0^{-1} corresponds to the local conformational transition rate.

(1) Conformational transitions should be accompanied with the damped vibrational motions observed by LAM-40. These motions assist distortions of degrees of freedom in the neighborhood of the conformation-transforming bond and keep the transition coordinate localized. The spatial scale of the damped vibrational motion has been evaluated as $\langle U^2\rangle^{1/2}$.

(2) We define the average rest time τ_0 for a conformation (lifetime of conformation) and the average jump time τ_1 between different conformations. Assuming $\tau_1 \ll \tau_0$, the rate of the conformational transition is given by τ_0^{-1}.

(3) The mean-square jump distance between different conformations is defined as $\langle l^2\rangle$. In the case of PB, we observe the jump motions of CH_2 or CH=CH as the conformational transition. In our measurements, the motions are detected through the motions of hydrogen atoms attached to the chain carbons, so that $\langle l^2\rangle^{1/2}$ corresponds to the jump distance of hydrogen atoms.

(4) As was shown in the simulation,[11] the degrees of freedom in the neighborhood of the conformation-transforming bond are distorted. It suggests that the average energy in the neighborhood increases due to the distortion, and bonds in the high energy state tend to cause conformational transitions. It is found in the computer simulation that cooperative transitions occur as well as isolated transitions. It is therefore considered that the transitions occur successively in the neighborhood of the previous transition. This succession leads to a physical picture of jump diffusion of the transition states. The diffusion is probably not long-wave behavior but damped in a finite distance. Such a damping effect is often introduced into models by a cut-off wavelength or a damping constant. However, we neglect it here because the Q range available for the analysis is restricted above 0.42 Å^{-1}.

(5) Strictly speaking, damped vibrational motions and conformational transitions are anisotropic, but in this model we assume that all the motions are isotropic.

The schematic sketch of the jump diffusion model with the damped vibrational motions is shown in Figure 7. This type of model has been generally formulated by Singwi and Sjolander.[24] According to them, the dynamic scattering law of this model $S_{jd}(Q,\omega)$ under the condition $\tau_0 \gg \tau_1$ is given by

$$S_{jd}(Q,\omega) = \frac{1}{\pi}\frac{\Gamma_{jd}\exp(-\langle U^2\rangle Q^2)}{\omega^2 + \Gamma_{jd}^2} \quad (4)$$

$$\Gamma_{jd} = \frac{DQ^2 + (1-\exp(-\langle U^2\rangle Q^2))/\tau_0}{1 + DQ^2\tau_0} \quad (5)$$

where D is the diffusion coefficient of transition site, given by $\langle l^2\rangle/6\tau_0$. $S_{jd}(Q,\omega)$ can be represented by a Lorentzian

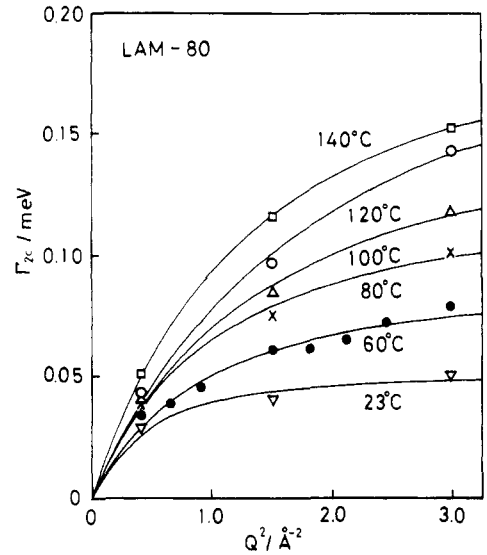

Figure 8. Q^2 dependence of half-width at half-maximum (hwhm) of the quasielastic component Γ_{2c} revealed by LAM-80; (▽) 23 °C; (●) 60 °C; (×) 80 °C; (△) 100 °C; (○) 120 °C; (□) 140 °C. Solid lines represent the best fits with eq 5.

with hwhm Γ_{dj}. This model describes only a single mode concerned with the local conformational transitions. In polymer systems, there are a number of very slow modes such as reptation motion. These slow motions do not give spectral broadening because of the limitation of the energy resolution of LAM-80, and therefore they are detected as a δ-function.[25,26] The damped vibrational motion observed by LAM-40 is also detectable with LAM-80 but is so broad compared with the energy window of LAM-80 that it is observed as a flat background. Taking into account these fast and slow motions, the dynamic scattering law observed by LAM-80 $S_{L80}(Q,\omega)$ can be expressed by

$$S_{L80}(Q,\omega) = S_{dv}(Q,\omega) \otimes [\{1 - A_{jd}(Q,\omega)\}\delta(\omega) + A_{jd}(Q)\, S_{jd}(Q,\omega)] \quad (6)$$

where $S_{dv}(Q,\omega)$ is the dynamic scattering law for the damped vibrations determined by LAM-40 (eq 2), $A_{jd}(Q)$ is a fraction of $S_{jd}(Q,\omega)$, and the symbol ⊗ means a convolution integral with ω. It should be noted that the Debye–Waller term due to the damped vibrational motion is involved in eq 6 through the convolution with $S_{dv}(Q,\omega)$. Assuming $\Gamma_{jd} \ll \Gamma_{1n}$ and Γ_{1b}, eq 6 can be reduced to

$$S_{L80}(Q,\omega) = C'(Q)[[1 - \{1 - A_{1n}(Q) - A_{1b}(Q)\}A_{jd}(Q) - A_{1n}(Q) - A_{1b}(Q)]\delta(\omega) + \{1 - A_{1n}(Q) - A_{1b}(Q)\}A_{jd}(Q) \times S_{jd}(Q,\omega) + A_{1n}(Q)\, L(Q,\omega,\Gamma_{1n}) + A_{1b}(Q)\, L(Q,\omega,\Gamma_{1b})] \quad (7)$$

Putting $\{1 - A_{1n}(Q) - A_{1b}(Q)\}A_{jd}(Q) = A_{2c}(Q)$ and $S_{jd}(Q,\omega) = S_{2c}(Q,\omega)$, eq 7 becomes identical with eq 3. The hwhm of the jump diffusion model Γ_{jd} (=Γ_{2c}) (eq 5) shows characteristic Q dependence. In the low Q limit, eq 5 becomes

$$\Gamma_{jd} = Q^2\{D + (\langle U^2\rangle/\tau_0)\} \quad (8)$$

Γ_{jd} is proportional to Q^2, showing diffusive behavior. On the other hand, in the high Q limit, it is given by

$$\Gamma_{jd} = 1/\tau_0 \quad (9)$$

In this region, the jump diffusion can be regarded as a localized motion. In Figure 8, the observed hwhm Γ_{2c} is plotted against Q^2 for 23, 60, 80, 100, 120, and 140 °C. Γ_{2c} is not proportional to Q^2 or independent of Q. This means that the Q dependence of Γ_{2c} can be approximated by neither the low Q nor the high Q limit. In order to evaluate

the parameters τ_0 and $\langle l^2 \rangle$ in the jump diffusion model, the Q dependent of Γ_{2c} is fitted in with the theoretical Γ_{jd} (eq 5). The mean-square amplitude $\langle U^2 \rangle$ evaluated from LAM-40 data was used as a fixed parameter. Solid lines in Figure 8 show the results of the fit. The agreement is good, and it is confirmed that the jump diffusion model is appropriate to describe the local conformational transitions. The values of τ_0 and $\langle l^2 \rangle$ are summarized in Table I where the diffusion coefficients D ($=\langle l^2 \rangle / 6\tau_0$) are also listed. The values of $\langle l^2 \rangle$ are almost independent of temperature, indicating that the mechanism of the local conformational transition does not change in the observed temperature range. On the other hand, the rest time τ_0 decreases with increasing temperature. The activation energy of τ_0 is estimated to be 2.9 kcal/mol from the Arrhenius plot of τ_0 in Figure 6b. This value is almost the same as the height of one barrier separating RIS but is slightly higher than that evaluated from the temperature dependence of Γ_{2c}.

Comparison with the Rate Theory. In this section, we will compare the rest time with Kramers' rate theory.[27] As mentioned before, Skolnick and Helfand[12] have extended Kramers' rate theory to multidimensional systems and evaluated the effect of the conformations on the transition rate. This procedure requires information of polymer conformations and interaction parameters. It is too difficult to get such information for the molten PB. In this discussion, we adopt the formalism of Kramers[27,28] to evaluate the rate of the local conformational transitions.

According to Kramers' theory, the conformational transition rate k_K is given by

$$k_K = \frac{(\gamma_A \gamma_B)^{1/2}}{2\pi\zeta}\left[\frac{1}{2} + \left(\frac{1}{4} + I_{\gamma_B}/\zeta^2\right)^{1/2}\right]^{-1} \exp\left(-\frac{E^*}{k_B T}\right) \tag{10}$$

where γ_A and γ_B are the curvatures of the potential at the bottom and the top, respectively, ζ is the friction coefficient of surrounding media, E^* is the potential barrier height, and $I = \sum m_i r_i^2$ is the moment of inertia of the rotating unit around a bond where m_i is the mass of the ith rotating unit and r_i is the distance from the rotation axis to the ith unit. In the molten PB system including no solvents, the observed activation energy (2.9 kcal/mol) is almost identical with one barrier height, suggesting that the effects of the friction coefficient ζ on the rate k_K is negligible. We assume that the conformational transition rate of molten PB can be described in the form of the low friction limit. It is given by

$$k_K = \frac{1}{2\pi}\left(\frac{\gamma_A}{I}\right)^{1/2} \exp\left(-\frac{E^*}{k_B T}\right) \tag{11}$$

In numerical calculation of the rate, k_K, the activation energy of τ_0 is employed as E^*, and γ_A is evaluated from $\partial^2 V(\theta)/\partial\theta^2$ assuming that the potential function $V(\theta)$ has the 3-fold form and can be expanded near the minimum; i.e.

$$V(\theta) = (E^*/2)(1 - \cos 3\theta) \simeq (9/4)E^*\theta^2 \quad \text{(near the minimum)} \tag{12}$$

The moment of inertia I is calculated based on the molecular structure of PB as shown in Figure 9. Assuming that CH_2 and CH=CH groups are individual units, we consider three types of the bond rotation, which have different moments of inertia. They are shown in Figure 10 where hydrogen atoms are eliminated for conciseness. For comparison with the observed conformational transition rate τ_0^{-1}, the moment of inertia I is averaged over

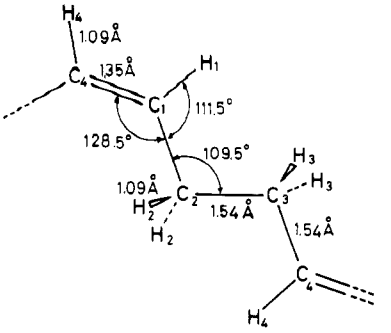

Figure 9. Structural parameters of *cis*-1,4-polybutadiene used in the calculation of conformational transition rate k_K of eq 11.

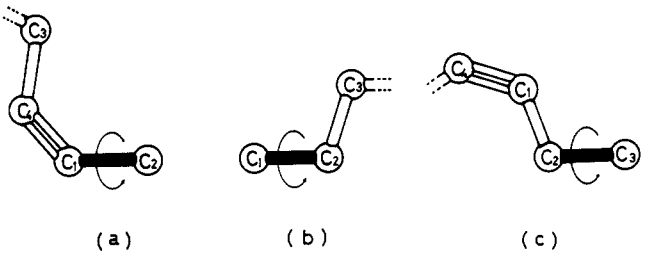

Figure 10. Three types of bond rotations that have different moments of inertia. In the figure, hydrogen atoms are eliminated for conciseness. Subscripts of C (1, 2, 3, and 4) correspond to those in Figure 9.

the three types of rotation weighted by the multiplicity of the rotations. The resulting average value $\langle I \rangle$ is 1.25×10^{-38} g cm^2. Using this value, we calculated the rate of the local conformational transition k_K and the corresponding rest time τ_K ($=k_K^{-1}$), which are summarized in Table I. The agreement between τ_0 and τ_K is very good; e.g., the observed value at 100 °C is 28.9 ps and the calculated one is 36.8 ps. The agreement may offer evidence that Kramers' theory at the low friction limit is appropriate for the description of the local conformational transitions of the molten PB. It should be noted that the excellent numerical agreement does not have very significant meaning because the rate calculated by the theory[12] is different by a factor 2–3 from that obtained by the simulation[11] even though the same model has been used.

Geometrical Consideration. The neutron-scattering measurements have been carried out as a function of scattering vector **Q** as well as of energy transfer ΔE. This provides geometrical or spatial information for the motions in addition to the time behaviors. The mean-square amplitude of the damped vibration $\langle U^2 \rangle$ and the jump distance $\langle l^2 \rangle$ have been evaluated based on the jump diffusion model. These observed quantities will be discussed from the viewpoint of molecular structure of PB in this section.

The amplitude $\langle U^2 \rangle$ should originate from vibrational motions near the potential minima. The softest mode or bond rotation mainly contributes to the amplitude $\langle U^2 \rangle$, so that assuming three-dimensional vibration it can be roughly given by

$$\langle U^2 \rangle \simeq \langle x^2 \sin^2 \Delta\phi \rangle \simeq \langle x^2 \rangle \sin^2 \langle \Delta\phi \rangle \tag{13}$$

where x is the distance from the rotational bond to hydrogen atom and $\Delta\phi$ the angular displacement from the potential minimum. The mean-square distance $\langle x^2 \rangle$ can be evaluated from the displacement of hydrogen atoms due to the bond rotations. We consider two bond rotations, C1–C2 and C2–C3 (see Figure 9), since C4–C3 rotation is identical with C1–C2 rotation. It is considered that following the rotation of C1–C2, not only the hydrogen

atoms H1 and H2 directly connected to C1 and C2, respectively, but also the H4 connected to C4 move because the C1=C4 bond does not rotate. As for the rotation of the C2–C3 bond, displacements of H2 and H3 are taken into account. By weighting with the number of hydrogens, we calculated the average value $\langle x^2 \rangle$ as 1.20 Å. The corresponding angular displacements $\langle \Delta\phi \rangle$ calculated from eq 13 are in the range from 33 to 42° for the temperature range 23–140 °C. The results are summarized in Table I. These values seem very large because $\langle \Delta\phi \rangle$ is 60° at the top of the potential barrier. Such large displacements make it easy that the local conformational transitions occur through a single bond rotation while the coordinate is localized.

Half of the jump distance $\langle l^2 \rangle^{1/2}$ can be also given from eq 13 by putting $\langle \Delta\phi \rangle = 60°$. In this calculation we include the displacements of hydrogen atoms that are affected by the conformational transitions. When a bond rotates for conformational transition, displacements of atoms or atomic groups occur on the left or right side of the bond. In the case of the rotation of C1–C2 in Figure 9, the displacements of H1 and C4 or H2 and C3, which are directly connected to C1 or C2, respectively, occur on the left or right side of the bond, respectively. According to the displacements of C4 and C3, H4 and H3 connected to C4 and C3, respectively, also move. The relative position of H4 to the C1–C2 bond does not change during the transition because the C4=C1 bond does not rotate. On the other hand, the relative position of H3 cannot be specified because of the C2–C3 rotation. The position of H3 is then represented by that of C3 in the calculation. As for the rotation of the C2–C3 bond, the displacements of H1 and H2 and H4 and H3 occur on the left and right sides of the bond, respectively. In the calculation, the relative positions of H1 and H4 to the C2–C3 bond are represented by those of C1 and C4, respectively, similar to the C1–C2 rotation. Averaging over three types of the rotations shown in Figure 10 and by weighting with the number of hydrogen atoms, we get $\langle l^2 \rangle_{cal}^{1/2} = 2.03$ Å. The agreement between the calculated and observed values is fairly good, suggesting the conformational transitions are mainly caused through a single bond rotation.

Our geometrical considerations are limited to at most the second neighboring bonds of the conformational transforming bond. The effects of the transitions should reach further bonds; the third and fourth neighboring bonds as indicated by the rate theory.[12] Furthermore, we consider only the torsional motions (bond rotation) neglecting the harder modes such as bond length stretching and bone angle bending. In practice, these modes also assist localization of the transitions. Regardless of these simplifications, the observed quantities can be well reproduced in the above calculations. We then believe that the torsional motions of the nearest and second neighboring bonds play the most important role for the local conformational transitions.

Conclusions

We have shown that there are two modes in the molten *cis*-1,4-polybutadiene in the time range 10^{-13}–10^{-10} s. The faster mode has been assigned to the damped vibrational motion and the slower one to the local conformational transitions. The local conformational transitions can be modeled by the jump diffusion motion accompanied with the damped vibrational motion. In conclusion, the results obtained by the model are summarized in Figure 11 in terms of potential representation along the reaction coordinate. The physical picture of the model agrees well with the results of the computer simulation by Helfand et al. This means that polymer chains are not so hard for the conformational transitions but softened by the vibrational motions, especially by the torsional motions. The softening is essential for the conformational transitions to occur through a single bond rotation and be localized.

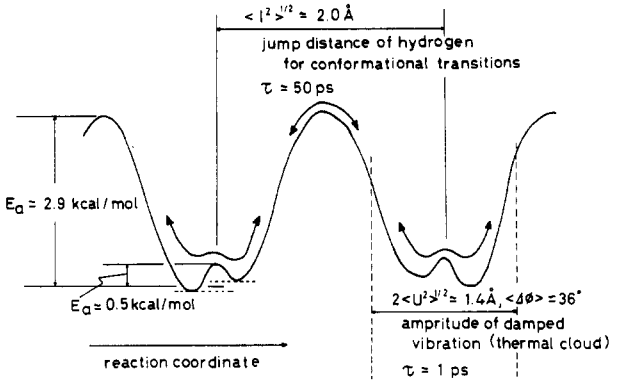

Figure 11. Schematic potential representation for local conformational transitions along the reaction coordinate.

References and Notes

(1) Schaeffer, J. *Macromolecules* **1973**, *6*, 882.
(2) Stockmayer, W. *Pure Appl. Chem.* **1976**, *15*, 539.
(3) Mashimo, S.; Nakamura, H.; Chiba, A. *J. Chem. Phys.* **1982**, *76*, 6324. Mashimo, S.; Yagihara, S.; Chiba, A. *Macromolecules* **1984**, *17*, 630.
(4) Bell, W.; North, A. M.; Pethrick, R. A.; Poh, B. T. *J. Chem. Soc., Faraday Trans. 2* **1979**, *75*, 1115.
(5) Viovy, J. L.; Melora, F.; Monnerie, L. *Macromolecules* **1985**, *18*, 1130. Viovy, J. L.; Frank, C. W.; Monnerie, L. *Macromolecules* **1985**, *18*, 2606. Viovy, J. L.; Monneri, L. *Polymer* **1986**, *27*, 181.
(6) Sasaki, T.; Yamamoto, M.; Nishijima, Y. *Macromolecules* **1988**, *21*, 610.
(7) Hyde, P. D.; Ediger, M. D.; Kitano, T.; Ito, K. *Macromolecules* **1989**, *22*, 2253.
(8) Liao, T. P.; Okamoto, Y.; Morawetz, H. *Macromolecules* **1979**, *12*, 535.
(9) Schatzki, T. F. *J. Polym. Sci.* **1962**, *57*, 496.
(10) Monnerie, L.; Geny, J. *J. Chim. Phys. Phys.-Chim. Biol.* **1969**, *66*, 1691.
(11) Helfand, E.; Wasserman, Z. R.; Weber, T. A. *J. Chem. Phys.* **1979**, *70*, 2016. Helfand, E.; Wasserman, Z. R.; Weber, T. A. *Macromolecules* **1980**, *13*, 526.
(12) Skolnick, J.; Helfand, E. *J. Chem. Phys.* **1980**, *72*, 5489.
(13) Helfand, E.; Wasserman, Z. R.; Weber, T. A.; Skolnick, J.; Runnels, J. *J. Chem. Phys.* **1981**, *75*, 4441.
(14) Allen, G.; Higgins, J. S.; Maconnachie, A. *J. Chem. Soc., Faraday Trans. 2* **1982**, *78*, 2117.
(15) Conversion of energy E to time t follows the relation $t = h/E = \nu^{-1}$, not $t = \hbar/E = \omega^{-1}$. In this paper, frequency is not represented by angular frequency ω but ν.
(16) Inoue, K.; Ishikawa, Y.; Watanabe, N.; Kaji, K.; Kiyanagi, Y.; Iwasa, H.; Kohgi, M. *Nucl. Instrum. Methods* **1984**, *A238*, 401.
(17) In *Polymer Handbook*, 3rd ed.; Brandrup, J., Immergut, E. H., Eds.; Wiley-Interscience: New York, 1989; Vol. 3.
(18) Bacon, G. E. *Neutron Diffraction*; Clarendon Press: Oxford, 1975.
(19) Springer, T. Quasielastic Neutron Scattering for the Investigation of Diffusive Motions in Solid and Liquids. *Springer Tracts in Modern Physics*; Springer-Verlag: Tokyo, Japan, 1972; Vol. 64.
(20) Hervet, T.; Vollino, F.; Dianoux, A. J.; Lechner, R. E. *J. Phys. Lett. (Paris)* **1974**, *35*, L-151.
(21) Vollino, F.; Dianoux, A. J. *Mol. Phys.* **1980**, *41*, 271.
(22) Buchenau, U.; Monkenbusch, M.; Stamm, M.; Majkrzak, C. F.; Nucker, N. Polymer Motion in Dense Systems. *Springer Proc. Phys.* **1988**, *29*, 138.
(23) Frick, B.; Richter, D.; Petry, W.; Buchenau, U. *Z. Phys. B* **1988**, *70*, 73.
(24) Singwi, K. S.; Sjolander, A. *J. Chem. Phys.* **1960**, *119*, 863.
(25) de Gennes, P.-G. *J. Phys. (Paris)* **1982**, *42*, 735.
(26) Ronca, P. F. *J. Chem. Phys.* **1983**, *79*, 1031.
(27) Kramers, H. A. *Physica* **1940**, *7*, 284.
(28) Helfand, E. J. *J. Chem. Phys.* **1971**, *54*, 4651.